# Surface Modification and Laser Pulse Length Effects on Internal Energy Transfer in DIOS

**Guanghong Luo,[†] Yong Chen,[†] Gary Siuzdak,[‡] and Akos Vertes*,[†]**

*Department of Chemistry, Institute for Proteomics Technology and Applications, The George Washington University, Washington, D.C. 20052, and Center for Mass Spectrometry, The Department of Molecular Biology, The Scripps Research Institute, La Jolla, California 92037*

*Received: August 3, 2005; In Final Form: October 5, 2005*

Benzyl-substituted benzylpyridinium (BP) chloride salts were used as a source of thermometer ions to probe the internal energy (IE) transfer in desorption/ionization on porous silicon (DIOS). To modify their wetting properties and the interaction energies with the thermometer ions, the DIOS surfaces were silylated to produce trimethylsilyl- (TMS), amine- (NH2), perfluoroalkyl- (PFA), and perfluorophenyl-derivatized (PFP) surfaces. Two laser sources—a nitrogen laser with pulse length of 4 ns and a mode locked $3 \times \omega$ Nd:YAG laser with a pulse length of 22 ps—were utilized to induce desorption/ionization and fragmentation at various laser fluence levels. The corresponding survival yields were determined as indicators of the IE transfer and the IE distributions were extracted. In most cases, with increasing the laser fluence in a broad range ($\sim$20 mJ/cm$^2$), no change in IE transfer was observed. For ns excitation, this was in remarkable contrast with MALDI, where increasing the laser fluence resulted in sharply (within $\sim$5 mJ/cm$^2$) declining survival yields. Derivatization of the porous silicon surface did not affect the survival yields significantly but had a discernible effect on the threshold fluence for ion production. The IE distributions determined for DIOS and MALDI from α-cyano-4-hydroxycinnamic acid reveal that the mean IE value is always lower for the latter. Using the ps laser, the IE distribution is always narrower for DIOS, whereas for ns laser excitation the width depends on surface modification. Most of the differences between MALDI and DIOS described here are compatible with the different dimensionality of the plume expansion and the differences in the activation energy of desorption due to surface modifications.

## Introduction

Matrix-assisted laser desorption/ionization (MALDI) is widely established as a soft ionization method for mass spectrometry (MS) of biological and synthetic macromolecules. Increasingly, MALDI is becoming an enabling technique for proteomics, nucleic acid analysis, and synthetic polymer characterization.[1,2] Due to interferences between low mass analytes and the matrix ions produced in the <700 Da mass range, the efficacy of MALDI is limited. Furthermore, sample preparation in MALDI imposes other limitations due to solubility and cocrystallization requirements. Several alternatives were proposed to complement MALDI in the low mass range. The application of micro- and nanoparticles as a matrix showed promising results.[1,3−6] Recently, the possibility of quantum confinement effects on peptide ion yields has been demonstrated for 2 nm gold particles.[7] Nanotubes[8] as well as nanoscopic surface structures[9] were also investigated as desorption/ionization substrates. To date, the emerging method of desorption/ionization on porous silicon (DIOS) has exhibited the most benefits.[10] The merits of DIOS include the lack of matrix interferences, simple spectra, and excellent sensitivity.[11]

The DIOS method utilizes photoelectrochemically etched silicon wafer to facilitate desorption.[10] The porous structure on the silicon surface efficiently absorbs energy from the incident laser pulse and induces desorption/ionization. In porous silicon (pSi), due to the moderate 30−40% porosity of the surface layer the absorption edge of bulk crystalline Si at $\sim$1.1 eV is blue-shifted by a few hundred meV. Thus, a wide array of laser sources are available for excitation in DIOS.[12]

The properties of pSi depend on the etching conditions, such as the concentration of the HF solution, the etching time, the applied current density, and the properties of the silicon wafer. For the typical n-type DIOS surfaces, the pore diameter distribution spans from nano- (<2 nm) to meso-scale (2−50 nm) and the porosity is 30−40%. The pore morphology depends on preparation conditions but high aspect ratio structures are typical. Structures with $\sim$10 nm pore diameter can exhibit pore lengths in excess of 1 $\mu$m.[13] The structure of electrochemically etched pSi was described as an assembly of quantum wires[14] or crystalline silicon nanoparticles[15] embedded in amorphous silicon and/or oxide. During the etching process, some other surface species, such as hydrides, oxyhydrides, and oxides are also formed.[15] The low end of the nanowire and nanoparticle size distribution (<5 nm) exhibits quantum confinement effects resulting in enhanced optical absorption. At the laser wavelength, optical absorption also occurs at the surface/interface defect states, e.g., nonbridging oxygen hole centers, in the porous layer and near the surface of the bulk silicon substrate. Close to the surface the absorption includes excitation of the electrons from the valence band to surface states and impurity holes with an absorption center near 3.0 eV.[16] The porous nature of the surface layer results in a high absorption cross section. At the nitrogen laser wavelength of 337 nm, an effective absorption coefficient of up to $10^5$ cm$^{-1}$ can be observed.[17]

The high surface area (hundreds of m$^2$/cm$^3$) of pSi enables the adsorption and storage of the analyte and solvent molecules.

* Address correspondence to this author: 725, 21st Street, N.W., Washington, D.C. 20052. Phone: (202) 994-2717. Fax: (202) 994-5873. E-mail: vertes@gwu.edu.

[†] The George Washington University.

[‡] The Scripps Research Institute.

10.1021/jp054311d CCC: $30.25 
Published on Web 12/06/2005

The distribution of the analyte inside the pores is determined by the wettability of the surface. The native pSi surface is terminated by Si−H bonds that are hydrophobic. This surface, however, is not stable and if left untreated in air it gradually oxidizes. Both the stability and the wettability of the pSi surface can be changed by oxidation and/or derivatization. Furthermore, the derivatization alters the interaction energy between the surface and the adsorbed analyte.

Ion formation in DIOS is thought to include two stages: desorption and ionization. Initially, the pSi substrate absorbs the laser energy and its temperature rises. As a consequence, the adsorbate desorbs from the surface and the solvent trapped in the pores (accentuated by capillary condensation) evaporates. This latter process can take the form of surface evaporation as well as spinodal decomposition. Due to the confinement imposed by the porous structure, the resulting plume cannot expand freely. Instead a quasi-one-dimensional expansion ensues that, compared to free expansion, retains plume density elevated for a longer period. Within a few ns the estimated surface temperature could be as high as 600 K, which could lead to rapid evaporation or, in the case of trapped solvents, spinodal decomposition.[18] The solvent residues trapped in the nanopores also experience a confinement effect. This leads to very large long-range density fluctuations and may induce a transition from bulk liquid to a two-dimensional adsorbate phase.[19]

The ionization mechanism in DIOS is largely unclear as several possible pathways can lead to ionization. Competing chemical reactions between the silicon substrate and the analyte, such as electron transfer to and from the surface and/or proton transfer from the excited Si−H groups to the analyte, can result in ion production.[10,20] The presence of hydrides (Si−H) and oxyhydrides (Si−O−H) in the structure creates surface states with sub-gap energy levels that open additional channels and also serve as a source of protons for ionization.[21] In some cases, preexisting ions or ion pairs can be present in the nanopores. Due to the electric fields from the accelerating voltage and the local fields from the laser beam, these ions can be separated and released from the surface.[18] Yet another possibility is that the trapped solvent and residual gas accumulated in the pores serve as photochemical ionization agents. At the introduction of residual acetic acid or water vapor, an ion yield enhancement of 10 to 40 times demonstrated that the gas-phase processes played a significant role in ionization.[18]

The morphology of the porous layer influences several factors in DIOS. Quantum confinement in the silicon structures between the fine pores supports exciton formation and enhances ionization. Depending on the wettability, these small pores may not be accessible for the analyte.[12] At the same time, the increased surface area due to the nanopores leads to additional adsorption of residual gases and contaminants and also promotes ionization.

Other properties of pSi such as its wettability and the interaction energy between the surface and the analyte also play a significant role in both desorption and ionization. Higher wettability results in more complete penetration of the analyte solution into the pore structure. The energy barrier for the analyte release from the surface controls the rate of desorption. This can be characterized by the activation energy of desorption, $E_a^{des}$, and by an Arrhenius-type rate coefficient for the desorption, $k_{des}$:

$$k_{des} = A \exp\left(-\frac{E_a^{des}}{RT}\right) \quad (1)$$

where the $A$ preexponential factor is considered to be the frequency of attempts to cross the barrier. The activation energy of desorption depends on the interactions between the surface and the adsorbate molecules as well as the surface coverage because of possible interactions between the adsorbates.

Modifications of the pSi surface by derivatization change both the polarity and the density of the surface molecules. Bulky organic molecules at the interface can change the distance between the adsorbate and the surface. In this study, we modify the properties of the pSi surface by derivatization with different organic molecules to change both the activation energy of desorption and the wettability. The presence of surface modifications can also influence the local phonon density and, thus, change the rate of energy transfer from the pSi to the adsorbate. The resulting differences in energy transfer are monitored through the yield of ion fragmentation reactions.

The IE transfer in "soft" ionization techniques, e.g., electrospray ionization (ESI) and MALDI, can be determined by using a series of so-called thermometer ions.[22,23] After determining the survival yield of their molecular ions, the mean IE of the generated ions and in some cases the IE distribution can be extracted by using the Rice−Ramsperger−Kassel−Marcus (RRKM) theory of unimolecular decomposition. In previous studies, benzyl-substituted benzylpyridinium salts and a benzyltriphenylphosphonium salt were used as thermometer ions to follow the IE of the ions produced in MALDI.[23,24] We found that the IE depended on the organic matrix, the laser fluence, and the laser pulse length. In MALDI, the complex collision dynamics in the matrix plume during expansion and the ion−molecule reactions between the matrix and analyte species determine the IE content of the emerging ions.

In DIOS, however, the dynamics can be very different because the desorption event is related to the interaction between the nanoporous Si surface and the analyte. Thus, the adsorbate−surface interaction energy is expected to influence the energy transfer during the desorption event. Changing the nature of this interaction through surface derivatization and measuring the IE of the desorbed species in this study is expected to give insight into the mechanism of the desorption event. Investigating the effect of laser fluence and pulse length on the IE transfer provides further information on the fundamental processes involved.[25]

Parametric studies of DIOS are underway. Investigations of the effect of laser wavelength, crystallographic orientation, preparation conditions, and other physical properties of the pSi (pore morphology, and thermal and optical properties) on ion generation help in the optimization of desorption conditions.[12,26,27] In these experiments, the laser wavelength (266, 355, and 532 nm), the mode of ion detection, and the pH of the sample solution were identified as significant factors. Further studies proved that the porosity and wetting properties of the pSi substrate played a major role in determining DIOS ion yields but some of the unique optical properties of the surface, i.e., luminescence, had no effect.[12]

To better understand the fundamental processes in DIOS, information on the coupling of energy from the laser to the substrate and to the adsorbate is needed. In addition to energy deposition, the dynamics of the plume, ionization mechanisms, and energy transfer between the surface and the adsorbate have to be explored. In this contribution, we present our efforts to follow the IE content of the desorbed ions as a function of the fluence and pulse length of the laser, and the chemical modifications of the silicon surface. To separate the energy transfer during desorption from the energy exchange associated with the ionization processes, the preformed thermometer ions

were used in this study. The radical cations of the benzyl-substituted benzylpyridinium chloride salts were already present in the solid phase. A comparison with similar data in MALDI reveals important differences between the two methods.

## Experimental Section

**Materials.** Acetonitrile and methanol were purchased from Fisher Scientific (Springfield, NJ) in HPLC grade quality. Deionized water (18.2 MΩ cm) was produced in-house using an E-pure system (Barnstead, Dubuque, IA). For surface derivatization, *N*,*O*-bis(trimethylsilyl)trifluoroacetamide (BSTFA) with 1% trimethylchlorosilane as catalyst and (3,3,4,4,5,5,6,6,6-nonafluorohexyl)chlorosilane (FHCS) and for MALDI α-cyano-4-hydroxycinnamic acid (CHCA) were obtained from Sigma Chemical Co. (St. Louis, MO). (3-Aminopropyl)-dimethylethoxysilane (APDMES) and (pentafluorophenyl)-propyldimethylchlorosilane (PFPPDCS) were purchased from Gelest, Inc. (Morrisville, PA). The benzyl-substituted benzylpyridinium (BP) chloride salts, 4-chloro- (4C), 4-fluoro- (4F), 4-methoxy- (4MO), 3-methoxy- (3MO), 4-methyl- (4M), 3-methyl- (3M), and 2-methyl- (2M), were synthesized and certified as reagent grade by Celestial Specialty Chemicals (Nepean, Ontario, Canada).

**Porous Silicon Preparation and Surface Modifications.** The details of surface preparation and modifications were presented elsewhere.[11] Briefly, low-resistivity (0.005−0.02 Ω cm) n-type Si(100) wafers were etched photoelectrochemically and oxidized by exposure to ozone. Subsequently, four different surfaces were prepared by derivatization, using BSTFA with 1% TMCS as a catalyst and APDMES, FHCS, and PFPPDCS as silylating reagents. These modifications produced trimethylsilyl- (TMS), amine- (NH2), perfluoroalkyl- (PFA), and perfluorophenyl-derivatized (PFP) surfaces, respectively. Sections of these plates were attached to the MALDI sample probe by double sided conductive carbon tape.

**DIOS-MS Experiments.** Detailed descriptions of the experimental setup and the protocol for IE determination were provided in our previous papers.[23,24] In these experiments, the BP chloride salts were dissolved in 50% methanol at a concentration of ∼70 μM. From this solution, 0.5μL was deposited on the DIOS plate and air-dried at ambient temperature. A nitrogen laser (VSL-337ND, Laser Science Inc., Newton, MA) with 337 nm wavelength and 4 ns pulse length and a mode locked 3 × ω Nd:YAG laser (PL2143, EKSPLA, Vilnius, Lithuania) with 355 nm wavelength and 22 ps pulse length were used for "ns" and "ps" excitation, respectively. Microscope inspection of the burn marks on photographic paper in the focal spot indicated that the fluence distribution was Gaussian for both lasers. The dimensions of the slightly elliptical focal area were 93 μm × 97 μm and 53 μm × 57 μm for the ns and the ps laser, respectively. For each sample, the laser was running at 2 Hz repetition rate with fluence levels selected in the range slightly above the ionization threshold. A low-pass optical filter was inserted into the beam-path of the "ps" laser to reject the residual output of the second harmonic at 532 nm. The ion current corresponding to the molecular and fragment ions was integrated in time and the survival yield, SY, was calculated:

$$\mathrm{SY} = \frac{\int_{\mathrm{M}} I_{\mathrm{M}}(t)\,\mathrm{d}t}{\int_{\mathrm{M}} I_{\mathrm{M}}(t)\,\mathrm{d}t + \int_{\mathrm{F}} I_{\mathrm{F}}(t)\,\mathrm{d}t} \qquad (2)$$

where $I_{\mathrm{M}}(t)$ and $I_{\mathrm{F}}(t)$ are the molecular ion (including both $M^+$ and $[M + H]^+$) and the fragment ion currents, respectively.

**Surface Imaging.** Atomic force microscopy (AFM) measurements were conducted to examine the morphology of the derivatized DIOS surfaces. Contact mode AFM imaging was performed (Multimode Scanning Probe Microscope, Veeco Instruments Inc., Santa Barbara, CA) with a Nanoscope IIIa controller (Digital Instruments) and a silicon nitride tip (Nanoprobe SPM NP-20, Veeco Instruments Inc., Santa Barbara, CA). The nominal tip radius was 20 nm and the front, back, and side angles were all 35°. Due to the geometry of the tip, it was not possible to image inside the narrow vertical channels in pSi. Only the entrance of some larger pores at the surface was visible.

**Internal Energy Distributions.** For each surface, the survival yields for the molecular thermometer ions obtained at comparable fluence levels were plotted as a function of the corresponding critical energy, $E_0$ (plot not shown). The critical energy is defined as the minimum energy that yields a nonzero rate coefficient for a unimolecular decomposition reaction. The SY vs $E_0$ data were fitted with a Boltzmann-type sigmoidal curve, $\mathrm{SY} = 1 - [1 + \exp(E_0 - E^*)/\Delta E]^{-1}$, where $E^*$ is the center and $\Delta E$ is the width of the distribution. Typically excellent fit was found with a correlation coefficient of $R > 0.97$ and all fits produced $R > 0.95$. The first derivative of this curve is reported as the internal energy distribution[22] for a specific laser and surface combination. It should be noted that this IE distribution does not include the correction due to the kinetic shift. Thus, the mean IEs are shifted compared to the values determined by inverting the Rice−Ramsperger−Kassel−Marcus (RRKM) unimolecular decomposition rate coefficients.[23]

## Results and Discussions

**Mass Spectral Features.** Mass spectra of all the substituted BP salts were taken on the four DIOS surfaces with both the ns and the ps laser. A representative spectrum of 4-methylbenzylpyridinium chloride shown in Figure 1a confirms that there are no matrix interferences. The absence of matrix peaks in the *m*/*z* 100−500 range allowed for an accurate determination of the yields for thermometer ions and their fragments, $F^+$. In the fluence range of interest, all thermometer ions showed efficient fragmentation indicating that the critical energy of unimolecular decomposition for these ions was comparable to the energy transfer in the desorption process. The threshold fluence for molecular ion formation coincided with the threshold for the appearance of fragment ions. In many spectra sodium and potassium ions appeared probably originating from the processed silicon or solvent impurities. No alkaline adducts of the thermometer ions or silicon related ions were observed. Due to the low fluence required for DIOS, laser ablation of silicon did not occur, but at very high fluences (>100 mJ/cm$^2$ for the ns laser), background peaks in the *m*/*z* 70 to 80 range were observed.

The inset in Figure 1a shows that in the molecular ion region both the radical cations and their hydrogen adducts were present. As the BP compounds are chloride salts, the radical cations are present already in the adsorbate phase. The formation of the hydrogen adducts can proceed either through neutralization via electron capture followed by protonation or by direct attachment of hydrogen atoms to the cations. Both the radical cation, $M^+$, and the hydrogen adduct, $[M + H]^+$, originate from the preformed $M^+$ ions in the solid phase. Thus, the preformed $M^+$ can be viewed as the precursor of all the $F^+$ fragment ions. An important feature of the porous substrate is that the laser plume produced inside the pores is initially spatially confined (see Figure 1c). This confinement enhances even the relatively low cross section reactions in the plume.

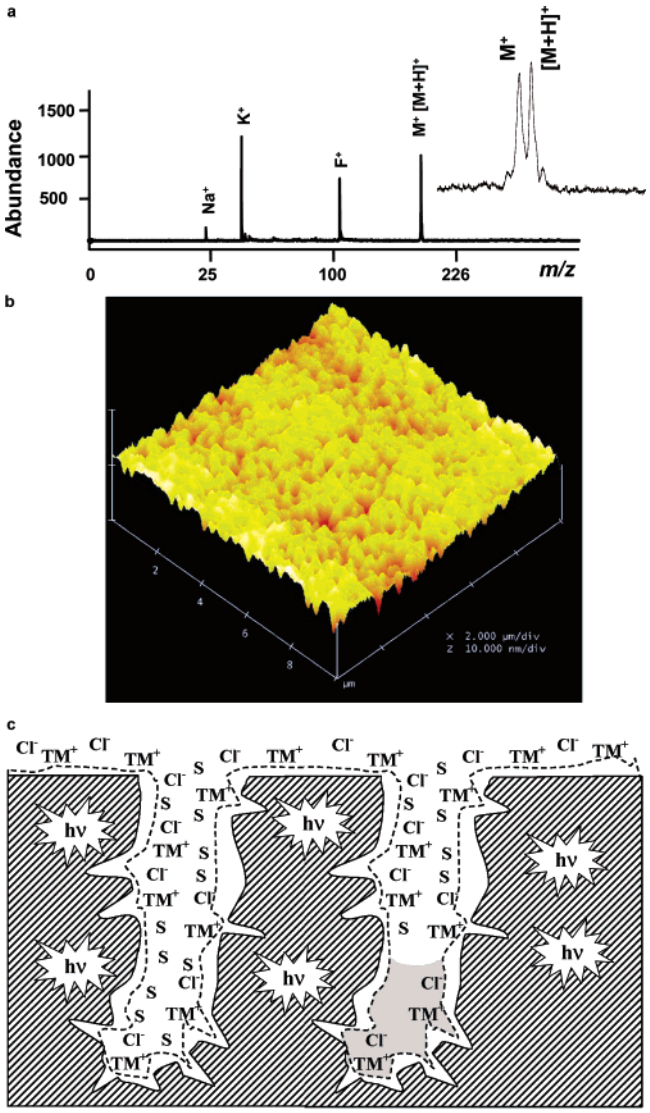


**Figure 1.** (a) Mass spectrum of 4-methylbenzylpyridinium chloride desorbed from a PFA-derivatized surface with use of a nitrogen laser shows a single fragment ion, $F^+$. Molecular ions are present as both radical cations, $M^+$, and hydrogen adducts, $[M + H]^+$ (see inset). Although compared to MALDI the source of $H/H^+$ is much reduced (no matrix), approximately the same level of H adduct formation is observed. (b) Topography of a $10 \times 10$ $\mu$m part of the DIOS surface from AFM measurements. Considering that the tip curvature is 20 nm, the image indicates that a significant number of the pore entrances are smaller in diameter. (c) Adsorption of thermometer molecular ions ($TM^+$ and $Cl^-$) and solvent molecules (S) in derivatized silicon nanopores. Derivatization is depicted as a dashed line that follows the surface. Pore walls are sufficiently thin to induce quantum confinement of electrons leading to enhanced absorption of laser light. The left pore only contains adsorbates and it is used to demonstrate the "dry" desorption mechanism. The right pore shows trapped solvent as a result of capillary condensation or inefficient pumping through nanopore (gray area) and exhibits a "wet" desorption mechanism.

**Surface Imaging.** Figure 1b represents the topography of a $10 \times 10$ $\mu$m part of the DIOS surface from AFM measurements. In this figure the entrances to some of the larger pores in the size distribution can be seen. Considering that the tip curvature is 20 nm, the image indicates that a significant number of the pores are smaller in diameter. The images of the pores with lateral features comparable to the tip curvature appear as a convolution of the tip and pore entrance shapes. Overall, the number of larger pores is fairly limited, thus one can assume that the majority of the pores are in the size range below the tip curvature.

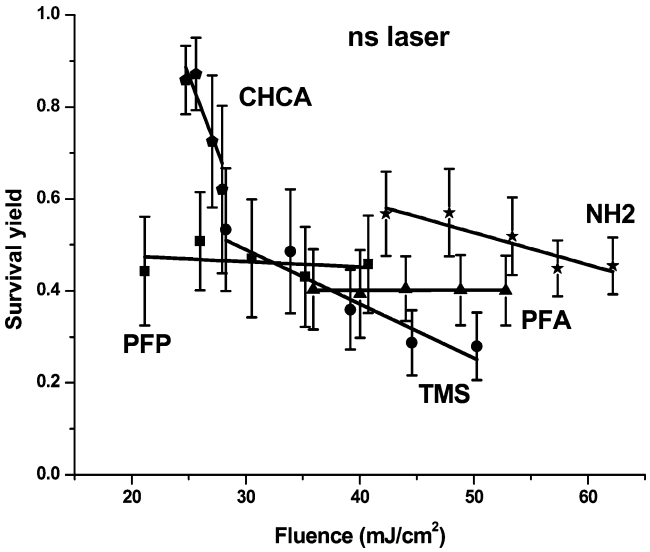


**Figure 2.** Comparison of survival yields for 3-methoxybenzylpyridinium ions desorbed from four different DIOS surfaces with a 4 ns pulse width nitrogen laser. Results for MALDI experiments with CHCA matrix are also included. Nonpolar surfaces derivatized with PFPPDCS require the lowest fluence, whereas the polar APMES surface produces ions at higher laser fluence. Survival yields are uniformly lower than in MALDI with CHCA matrix and show less pronounced fluence dependence.

**Survival Yield Measurements with the ns Laser.** The variation of the survival yield with laser fluence for 3MO-BP on the four derivatized DIOS surfaces is illustrated in Figure 2. For comparison, the corresponding MALDI results are also plotted. For the TMS surface, increasing the laser fluence resulted in slightly declining survival yields, but for the other surfaces there was no change in the studied fluence range. Linear regression provides $-0.012$, $-0.007$, $-0.001$, and $0.000$ cm$^2$/J for the slopes of TMS, NH2, PFP, and PFA surfaces, respectively. In contrast, survival yields in MALDI from the CHCA matrix show a sharp decline with increasing laser fluence. The slope obtained for this case is $-0.065$ cm$^2$/J. Although survival yields in DIOS are significantly lower, the values are practically unchanged in a broad fluence range. While meaningful MALDI data were only obtained in a $\sim$5 mJ/cm$^2$ range, for DIOS a range of $\sim$20 mJ/cm$^2$ yielded results. This observation, in combination with the different slopes of the survival yield vs fluence relationship, indicates some fundamental differences in the corresponding mechanisms. While in MALDI increasing laser fluence leads to an increase in energy transfer, it appears that in DIOS the energy transfer is independent of the fluence.

A possible explanation of such an effect can be given in terms of the energy transfer bottleneck models for heterogeneous[28] and homogeneous systems.[29] In MALDI the analyte molecules are embedded into the strongly absorbing molecular matrix. Upon laser excitation, a plume of matrix and analyte molecules is formed. For the duration of the laser pulse, the matrix including the plume continues to absorb energy. As the hot matrix molecules travel with the analyte the energy exchange continues until the ion−molecule collisions cease due to the expansion. In the "dry" desorption mechanism of DIOS, however, the energy is deposited into the silicon pore walls. Due to the rapid heating of the surface, the analyte and solvent molecules are desorbed from the energy absorbing silicon and leave the hot surface behind (see the *left pore* in Figure 1c). This gives rise to a low-density plume that propagates against

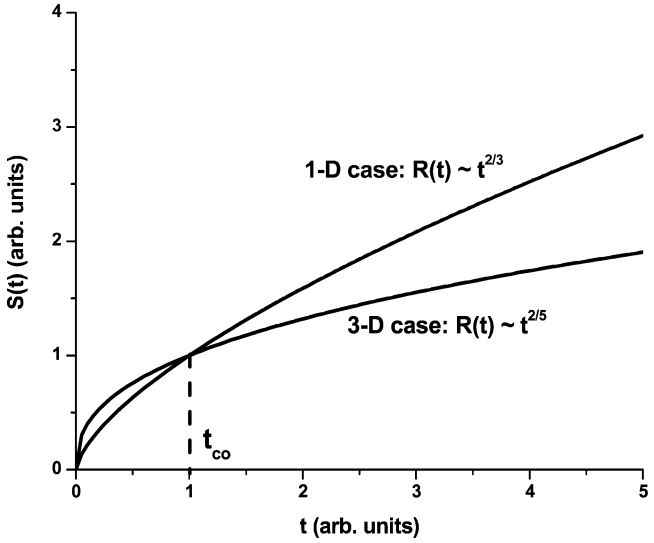


**Figure 3.** Comparison of shock front kinetics for 1D and 3D expansion. Initially the 3D expansion is faster but after the crossover time, $t_{co}$, the 1D expansion takes over.

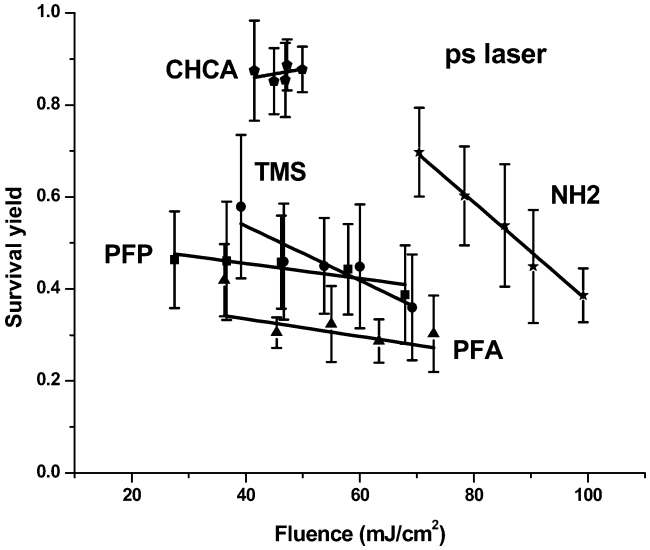


**Figure 4.** Survival yield data for 3MO-BP ions desorbed with a 22 ps pulse length mode locked $3 \times \omega$ Nd:YAG laser. Four different DIOS surfaces are compared with MALDI experiments with CHCA matrix. With ps laser excitation survival yields are significantly lower in DIOS than in MALDI.

the background gas pressure in the pores and a weak shock wave is generated. Although both in MALDI and in DIOS there is an energy transfer bottleneck (due to the frequency mismatch between the surface phonon modes and the intramolecular vibrations), in DIOS the energy transfer is further limited due to the reduced interaction time between the analyte species and the hot surface. This limitation might result in a more uniform survival yield in DIOS.

Depending on the surface wettability, there is a different potential scenario termed "wet" desorption mechanism which is depicted in the *right pore* in Figure 1c. While the left pore only contains adsorbates of the thermometer ions and solvent, the right pore also shows trapped residues of liquid solvent (e.g., water). The presence of this liquid phase in a vacuum environment can be explained either by the dramatically enhanced capillary condensation in the nanopores[30] or by the vastly reduced pumping speed through the constriction of these pores. In the presence of such a phase, rapid heating by the pore walls results in superheating and spinodal decomposition (phase explosion) of the liquid. The development of a dense solvent plume leads to a strong shock wave propagating against the background gas pressure in the pores. This higher plume density distinguishes the desorption in the right pore ("wet" desorption) from that in the left pore ("dry" desorption).

In either of these scenarios, due to the high aspect ratio of the pores in DIOS (1 $\mu$m/10 nm $\approx$ 100) the expansion of the desorbed plume is confined to a quasi-one-dimensional (1D) regime. This is in sharp contrast to the three-dimensional (3D) expansion in MALDI. Due to the different dimensionality, the displacement of the shock front, $S(t)$, exhibits different kinetics:[31]

$$S(t) = \lambda_d \left(\frac{E}{\rho_d}\right)^{1/(2+d)} t^{2/(2+d)} \qquad (3)$$

where $d$ is the dimension of the expansion, $E$ is the deposited energy, $\rho_d$ is the density of the $d$-dimensional environment, and $\lambda_d$ is a dimension-dependent constant. Comparing the 1D and 3D expansion reveals a crossover at time $t_{co} = (\lambda_3/\lambda_1)^{15/4}(\rho_1^5/\rho_3^3)E^{-1/2}$ (see Figure 3) in the temporal behavior. Initially, the radius of the 3D expansion exceeds the displacement of the 1D case, which, in turn, means lower density in the 3D expansion. This also means that the reactions in the early phase of the plume expansion proceed at a higher rate in the 1D case due to the higher densities in the confined environment. From the expression for $t_{co}$ it is also clear that decreasing the background gas density (or increasing the energy) leads to earlier crossover. Conversely, increasing the residual gas pressure $\rho_1$ (like in the experiments described in ref 18) prolongs the duration of relatively higher density plume in the 1D case. Higher collision rates in this 1D plume also explain more efficient energy transfer within the plume and, as a consequence, lower survival yields.

**Derivatization Effects.** Although the surface modifications did not have a major impact on the survival yields, they had a discernible effect on the threshold and the range of fluence values that resulted in ion production. The PFP modified DIOS surface required the lowest fluence threshold to initiate ionization and, practically simultaneously, fragmentation. Figure 2 demonstrates this for the 3MO-BP ions but similar results were obtained for the other six thermometer ions.

The large effect of derivatization on the threshold fluence, e.g., changing from 21 mJ/cm$^2$ for the hydrophobic PFP surface to 42 mJ/cm$^2$ for the hydrophilic NH2 surface in the case of 3MO-BP, shows that the activation energy of desorption for the ionic thermometer species indeed increases with the increase in the polarity of the surface. Changing the activation energy of desorption, however, does not result in appreciable change in survival yields. The insensitivity of DIOS survival yields in a wide fluence range to surface modifications indicates that the IE transfer is likely governed by plume processes.

**Laser Pulse Length Effects.** Figure 4 illustrates the survival yields of 3MO-BP for ps laser excitation on the four DIOS surfaces and in MALDI. While the general trends are similar to ns excitation (see Figure 2), there are some noticeable differences.

Both ns and ps excitation yield much lower survival yields in DIOS than in MALDI. The available fluence ranges are significantly broader for DIOS in both cases, although generally ps excitation requires somewhat higher fluences to obtain the same ion yields. For both lasers, the hydrophobic PFP surface produces ions at the lowest fluence, whereas the hydrophilic NH2 surface requires the highest fluence. The similar desorption characteristics in DIOS point to the similarities in energy

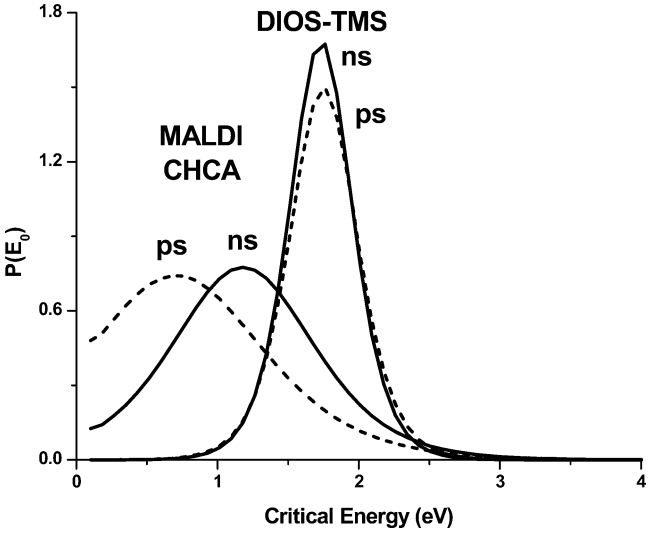


**Figure 5.** Comparison of internal energy distribution of thermometer ions desorbed from TMS derivatized DIOS surfaces and from CHCA matrix in MALDI, using "ns" (solid lines) and "ps" (dashed lines) laser excitation. MALDI data were obtained at 25.6 and 45.2 mJ/cm$^2$ with the "ns" and "ps" laser, respectively. Corresponding fluences for DIOS were 52.4 mJ/cm$^2$ ("ns" laser) and 55.8 mJ/cm$^2$ ("ps" laser). Kinetic shifts are not reflected.

deposition. As the excitation of porous silicon occurs on the subpicosecond time scale,[32] the two pulse lengths used in this study (4 ns and 22 ps) are expected to result in comparable fluence thresholds for desorption. These observations are coherent with the simple qualitative model we put forward above.

Perhaps the most remarkable difference between the two excitation modes is in the sensitivity of MALDI survival yields to changes in laser fluence. While the decline in 3MO-BP survival yields in CHCA matrix is very pronounced for ns laser (the slope is $-0.065$ cm$^2$/J), in the case of ps excitation there is no such effect (the slope is 0.002 cm$^2$/J). This difference can be explained in terms of laser−plume interactions.[25] In MALDI the expanding matrix plume continues to absorb energy from the 4 ns laser pulse and the energy transfer to the thermometer ions persists as long as collisions are present. Thus, increasing fluence leads to declining survival yields. However, the 22 ps laser pulse ceases before significant matrix plume expansion takes place. Thus, during the expansion phase, no energy deposition takes place and as a consequence the survival yields remain unchanged with increasing fluence.

**Internal Energy Distributions.** By design, the different thermometer ions exhibit a range of critical energies. The purpose of this spread is to be able to probe the distribution of IEs in the desorption process. By using the method described in the Experimental Section, the IE distributions for the four DIOS surfaces and MALDI from CHCA were extracted for desorption experiments conducted by the two laser sources. A representative comparison is given in Figure 5. The data in this figure accentuate our earlier observations. It is further demonstrated that MALDI produces ions with lower IEs than DIOS. It can also be noticed that compared to ns excitation the ps laser in MALDI generates less energy transfer, whereas in DIOS such a difference is not observed. A new feature apparent from Figure 5 is the difference in the width of IE distributions; however, this is specific to the TMS surface (see below).

Further details of the IE distributions are revealed by Tables 1 and 2 in the case of ns and ps excitation, respectively. In these tables, the mean, $E^*$, and the width, $\Delta E$, of the IE distribution are shown together with the fluence used, $F$, and the squared correlation coefficient, $R^2$, of the fit for the studied systems. The $E^*$ and $\Delta E$ parameters are compared at the closest available fluence levels for the four DIOS surfaces and for MALDI from CHCA.

**TABLE 1: Center (without the Kinetic Shift) and Width of IE Distributions for Desorbed Ions in DIOS and MALDI with the "ns" Laser**

| "ns" laser | $F$ (mJ/cm$^2$) | $E^*$ (eV) | $\Delta E$ (eV) | $R^2$ |
|---|---|---|---|---|
| DIOS-TMS | 52.4 | $1.73 \pm 0.04$ | $0.14 \pm 0.05$ | 0.95 |
| DIOS-NH2 | 42.4 | $1.77 \pm 0.09$ | $0.36 \pm 0.16$ | 0.95 |
| DIOS-PFA | 52.7 | $1.76 \pm 0.05$ | $0.28 \pm 0.07$ | 0.98 |
| DIOS-PFP | 40.7 | $1.66 \pm 0.13$ | $0.37 \pm 0.20$ | 0.91 |
| MALDI-CHCA | 25.6 | $1.18 \pm 0.13$ | $0.33 \pm 0.10$ | 0.98 |

**TABLE 2: Center (without the Kinetic Shift) and Width of IE Distributions for Desorbed Ions in DIOS and MALDI with the "ps" Laser**

| "ps" laser | $F$ (mJ/cm$^2$) | $E^*$ (eV) | $\Delta E$ (eV) | $R^2$ |
|---|---|---|---|---|
| DIOS-TMS | 55.8 | $1.75 \pm 0.03$ | $0.16 \pm 0.04$ | 0.97 |
| DIOS-NH2 | 76.0 | $1.72 \pm 0.11$ | $0.21 \pm 0.24$ | 0.92 |
| DIOS-PFA | 72.9 | $1.86 \pm 0.04$ | $0.22 \pm 0.05$ | 0.99 |
| DIOS-PFP | 60.4 | $1.83 \pm 0.11$ | $0.23 \pm 0.14$ | 0.94 |
| MALDI-CHCA | 45.2 | $0.70 \pm 0.41$ | $0.41 \pm 0.16$ | 0.99 |

In MALDI from CHCA, a lower $E^*$ is found for all the studied distributions. Although in the case of the ns laser this could be the result of the lower fluence used in these experiments, looking at Figures 2 and 4 confirms that this is not the case. A possible explanation of this observation can be based on the differences in plume expansion dynamics due to the different dimensionality in DIOS and MALDI (see eq 3). If this explanation holds it can be concluded that in determining the IE of the desorption products the dimensionality of expansion matters more than the activation energy of desorption.

The difference between MALDI and DIOS in $\Delta E$ shown in Figure 5 holds true for all systems in the case of the ps laser. For the ns laser, however, only the TMS surface exhibits a significantly narrower IE distribution than MALDI. The other three DIOS surfaces, PFA, PFP, and NH2, produce IE distributions comparable in width to MALDI. From these observations one can conclude that both laser pulse length and surface modifications influence the width of the IE distributions.

## Conclusions

Controlled fragmentation of the analyte in the MS of biomolecules is a prerequisite for their structural identification. Soft desorption ionization methods, such as soft laser desorption, produce molecular ions with varying amounts of IE, which leads to variations in the degree of fragmentation. The two fundamental steps in this process, desorption and ionization, contribute to the IE content in different ways. While IE transfer due to desorption is usually kinetically controlled, the contribution from ionization processes is determined by the thermodynamics of the ionization step. In this paper, we eliminated the ionization step by using preformed ions as analytes and uncovered the IE transfer due to only the desorption step.

Comparing the energy deposition in the desorption process during MALDI and DIOS revealed that the latter produced ions with higher energy content. Surprisingly, the IE depended much less on laser fluence in DIOS than in MALDI. Indeed, the degree of fragmentation, measured by the survival yield, was remarkably insensitive to laser fluence variations and to surface derivatization. This feature is important in the analytical applications of DIOS. Producing ions with reproducible IE

content means that the fragment ion yields are stable. This, in turn, enables reliable structural identification.

The substantial differences in IE transfer between MALDI and DIOS can be interpreted through several mechanistic distinctions. While the energy transfer in the MALDI plume is a homogeneous process (the matrix and analyte plumes expand together), in DIOS it is heterogeneous, i.e., the hot silicon surface is left behind by the desorbed analyte. Another major difference stems from the dimensionality of the expansion. Whereas the MALDI plume expands in three dimensions, the DIOS plume is confined in a narrow pore, thus its expansion is one-dimensional. In DIOS, both the lower dimensionality and the increased background pressure in the capillary pores result in slower expansion and elevated plume densities sustained for a longer time. Furthermore, the retention of liquid residues or capillary condensation in the pores contributes to higher plume densities. All these factors can account for the enhanced rates of protonation in DIOS demonstrated by the presence of protonated thermometer species even in the absence of an obvious source of protons. It is interesting to note that the above outlined mechanism can also explain why simple mechanical roughening of a polished silicon surface makes it a viable (but not efficient) soft laser desorption ionization substrate. The grooves and crevices created by abrasion can act similar to the pores observed in DIOS. Although these mechanistic considerations are compatible with our findings on IE transfer, they are by no means the only explanation. Further experiments are needed to establish the relative role of the contributing factors.

**Acknowledgment.** Insightful advice on this paper from Dr. A. Yergey of the National Institutes of Health is greatly appreciated. The authors are grateful for the financial support from the Chemical Sciences, Geosciences and Biosciences Division, Office of Basic Energy Sciences, Office of Science, U.S. Department of Energy (DE-FG02-01ER15129), the W. M. Keck Foundation (041904), and the George Washington University Research Enhancement Fund (GWU-REF). Support from the Department of Energy does not constitute an endorsement of the views expressed in the article.

## References and Notes

(1) Tanaka, K.; Waki, H.; Ido, Y.; Akita, S.; Yoshida, Y.; Yoshida, T. *Rapid Commun. Mass Spectrom.* **1988**, *2*, 151−153.

(2) Karas, M.; Hillenkamp, F. *Anal. Chem.* **1988**, *60*, 2299−2301.

(3) Sunner, J.; Dratz, E.; Chen, Y. C. *Anal. Chem.* **1995**, *67*, 4335−4342.

(4) Schürenberg, M.; Dreisewerd, K.; Hillenkamp, F. *Anal. Chem.* **1999**, *71*, 221−229.

(5) Han, M.; Sunner, J. *J. Am. Soc. Mass Spectrom.* **2000**, *11*, 644−649.

(6) Kinumi, T.; Saisu, T.; Takayama, M.; Niwa, H. *J. Mass Spectrom.* **2000**, *35*, 417−422.

(7) McLean, J. A.; Stumpo, K. A.; Russell, D. H. *J. Am. Chem. Soc.* **2005**, *127*, 5304−5305.

(8) Xu, S.; Li, Y.; Zou, H.; Qiu, J.; Guo, Z.; Guo, B. *Anal. Chem.* **2003**, *75*, 6191−6195.

(9) Cuiffi, J. D.; Hayes, D. J.; Fonash, S. J.; Brown, K. N.; Jones, A. D. *Anal. Chem.* **2001**, *73*, 1292−1295.

(10) Wei, J.; Buriak, J. M.; Siuzdak, G. *Nature* **1999**, *399*, 243−246.

(11) Trauger, S. A.; Go, E. P.; Shen, Z. X.; Apon, J. V.; Compton, B. J.; Bouvier, E. S. P.; Finn, M. G.; Siuzdak, G. *Anal. Chem.* **2004**, *76*, 4484−4489.

(12) Kruse, R. A.; Li, X. L.; Bohn, P. W.; Sweedler, J. V. *Anal. Chem.* **2001**, *73*, 3693−3645.

(13) Shen, Z. X.; Thomas, J. J.; Averbuj, C.; Broo, K. M.; Engelhard, M.; Crowell, J. E.; Finn, M. G.; Siuzdak, G. *Anal. Chem.* **2001**, *73*, 612−619.

(14) Canham, L. T. *Appl. Phys. Lett.* **1990**, 57, 1406.

(15) Cullis, A. G.; Canham, L. T.; Calcott, P. D. J. *J. Appl. Phys.* **1997**, *82*, 909−965.

(16) Brandt, M. S.; Fuchs, H. D.; Stutzmann, M.; Webber, J.; Cardona, M. *Solid State Commun.* **1992**, *81*, 307−312.

(17) Kovalev, D.; Polisski, G.; Ben-Chorin, M.; Diener, J.; Koch, F. *J. Appl. Phys.* **1996**, *80*, 5978−5983.

(18) Alimpiev, S.; Nikiforov, S.; Karavanskii, V.; Minton, T.; Sunner, J. *J. Chem. Phys.* **2001**, *115*, 1891−1901.

(19) Heuberger, M.; Zach, M.; Spencer, N. D. *Science* **2001**, *292*, 905−908.

(20) Ogata, Y. H.; Kato, F.; Tsuboi, T.; Sakka, T. *J. Electrochem. Soc.* **1998**, *145*, 2439−2444.

(21) Prokes, S. M.; Glembocki, O. J.; Bermudez, V. M.; Kaplan, R.; Friedersdorf, L. E.; Searson, P. C. *Phys. Rev. B* **1992**, *45*, 13788.

(22) Collettte, C.; Drahos, L.; De Pauw, E.; Vékey, K. *Rapid Commun. Mass Spectrom.* **1998**, *12*, 1673−16778.

(23) Luo, G. H.; Marginean, I.; Vertes A. *Anal. Chem.* **2002**, *74*, 6185−6190.

(24) Vertes, A.; Luo, G.; Ye, L.; Chen, Y.; Marginean, I. *Appl. Phys. A* **2004**, *79*, 823−825.

(25) Chen, Y.; Vertes, A. *J. Phys. Chem. A* **2003**, *107*, 9754−9761.

(26) Shen, Z. X.; Thomas, J. J.; Averbuj, C.; Broo, K. M.; Engelhard, M.; Crowell, J. E.; Finn, M. G.; Siuzdak, G. *Anal. Chem.* **2001**, *73*, 612−619.

(27) Lewis, W. G.; Shen, Z. X.; Finn M. G.; Siuzdak, G. *Int. J. Mass Spectrom.* **2003**, *226*, 107−116.

(28) Zare, R. N.; Levine, R. D. *Chem. Phys. Lett.* **1987**, *136*, 593−599.

(29) Vertes, A.; Gijbels, R.; Levine, R. D. *Rapid Comm. Mass Spectrom.* **1990**, *4*, 228−233.

(30) Gelb, L. D.; Gubbins, K. E.; Radhakrishnan, R.; Sliwinska-Bartkowiak, M. *Rep. Prog. Phys.* **1999**, *62*, 1573−1659.

(31) Sedov, L. I. *Similarity and Dimensional Methods in Mechanics*, 10th ed.; CRC Press: Boca Raton, FL, 1993.

(32) von Behren, J.; Kostoulas, Y.; Ucer, K. B.; Fauchet, P. M. *J. Non-Cryst. Solids* **1996**, *198*−*200*, 957−960.